

Medium-Range Order in High Al-content Amorphous Alloys Measured by Fluctuation Electron Microscopy

W.G. Stratton, J. Hamann, J.H. Perepezko, P.M. Voyles
Department of Materials Science and Engineering, University of Wisconsin – Madison
1509 University Avenue, Madison, WI 53706, U.S.A.

ABSTRACT

We have used fluctuation electron microscopy (FEM) to measure nanoscale medium-range order in amorphous $\text{Al}_{92}\text{Sm}_8$. Samples of this amorphous alloy formed by rapid quenching (melt-spinning) show a high density of pure Al nanocrystals ($>10^{20} \text{ m}^{-3}$) after low temperature ($< 250 \text{ }^\circ\text{C}$) devitrification. In samples amorphized by deformation (cold-rolling), primary Al-crystallization does not occur. This difference in devitrification behavior suggests an underlying structural difference in the amorphous state. FEM is a quantitative microscopy technique for determining nanoscale medium-range order in amorphous materials. Our measurements show that amorphous alloys formed by melt-spinning and cold-rolling have significant structural differences, and that annealing melt-spun alloy under conditions previously shown to modify the devitrification thermodynamics also changes the medium-range structure.

INTRODUCTION

High-Al content amorphous alloys [1, 2] exhibit very high tensile strength and unusual devitrification microstructure, the origin of which is not well understood. These amorphous alloys can be produced by rapid quenching from the melt or by mechanical deformation. The very high cooling rates required for rapid quenching are most often achieved by melt-spinning. A bulk ingot of the desired composition, often produced by arc-melting, is melted and ejected under pressure onto a metal wheel spinning at high speed in an inert atmosphere, producing a ribbon of amorphous alloy. As solidified high Al-content amorphous alloys have tensile strengths as high as $\sim 1000 \text{ MPa}$ [1].

Upon devitrification, these amorphous alloys exhibit primary crystallization of Al nanocrystals at an extremely high density in a amorphous matrix [3]. In melt-spun amorphous $\text{Al}_{92}\text{Sm}_8$, annealing at $< 250 \text{ }^\circ\text{C}$ produces pure Al nanocrystals at concentrations $>10^{20} \text{ m}^{-3}$ [4, 5]. These nanocrystals form from material with a higher solute concentration than the eutectic alloy of the system [6]. In other high-Al content amorphous alloys, partial crystallization increases the tensile strength to $\sim 1500 \text{ MPa}$ [1, 7].

Deformation-induced amorphization involves intense mechanical working of polycrystalline starting materials. This is often achieved by repeated cold rolling, which involves stacking elemental foils into a multi-layer sandwich with the desired composition and rolling it repeatedly at room temperature until it amorphizes. (See Ref [8] for a discussion of cold-rolling $\text{Al}_{92}\text{Sm}_8$.) In cold-rolled $\text{Al}_{92}\text{Sm}_8$ amorphous alloy, devitrification does not proceed by primary Al-crystallization [5].

While the high density of nanocrystals formed from the melt-spun alloy is attractive, the structural precursor of nanocrystal formation in the amorphous phase is uncertain. Large impurity concentrations can be avoided with appropriate processing, and x-ray diffraction

experiments show no second-phase crystals. Several alternatives with different implications for the atomic structure of the amorphous phase have been suggested, including quenched-in nuclei formed in the melt [4, 9] and amorphous phase separation [10, 11]. It has also been shown that annealing melt-spun material below the crystallization temperature modifies both the thermodynamics of primary crystallization and the resulting microstructure [12].

Taken together, this all suggests that the nucleation sites for primary crystallization in melt-spun $\text{Al}_{92}\text{Sm}_8$ amorphous alloy may be a form of nanometer length scale structural order, or medium-range order (MRO). Understanding the nature of this structure and how processing can modify it will be important to tailoring the devitrification of high Al-content amorphous alloy. The potential for deviations from a dense random packed structure in real amorphous alloy samples is also of significant fundamental interest.

Here we report initial results from experiments using fluctuation electron microscopy (FEM) to measure MRO in $\text{Al}_{92}\text{Sm}_8$ amorphous alloy. We have examined amorphous alloys prepared by melt-spinning and cold rolling and the effect of low-temperature annealing on MRO in the melt-spun material. These amorphous alloys exhibit different devitrification behavior, and we have found differences in their nanoscale structure.

FEM is a technique to quantitatively detect MRO in amorphous materials [13, 14]. FEM uses hollow-cone dark field imaging in a transmission electron microscope (TEM) to measure diffraction from nanoscale volumes of the sample. As we tilt the electron beam, pockets of structural order will meet a Bragg condition and strongly scatter electrons; an excited Bragg condition will generate a bright spot in a dark field micrograph compared to the amorphous matrix. If there are more ordered regions in the sample (more MRO), there will be more bright spots in the image. If the beam is tilted between Bragg conditions, the ordered pockets will appear particularly dark. Overall, the more speckle of bright and dark areas that appear in a dark field micrograph, the more MRO is present in the sample.

FEM uses a deliberately low image resolution of 1-2 nm in order to optimize the signal to noise of ordered structures in a disordered background. Ideally, we would match the resolution of the microscope to the size of the ordered region. Using a smaller volume reduces the signal from the ordered pockets, which is proportional to the square of the number of atoms in the pocket. A larger volume includes more disordered background material. The ability to make coherent kinematic diffraction measurements from volumes this small is unique to the electron microscope.

Even a completely random structure will have some variability in the image at the nanoscale, so FEM requires a quantitative measure of the degree of speckle. We chose a simple statistical measure, the normalized variance, defined as

$$V(k, Q) = \frac{\langle I^2(\mathbf{r}, k, Q) \rangle}{\langle I(\mathbf{r}, k, Q) \rangle^2} - 1, \quad (1)$$

where $I(\mathbf{r}, k, Q)$ is the image intensity as a function of position \mathbf{r} in the image, the dark field scattering vector magnitude k , and objective aperture size Q [14]. $V(k, Q)$ has been shown to depend on the three- and four-body atomic position correlation functions [15], unlike standard diffraction, which depends only on the pair correlation function. Peaks in $V(k)$ give information about the type of MRO from their position in k , and the degree of MRO from their magnitude.

The majority of FEM measurements to date have been on elemental amorphous semiconductor thin films [13, 14, 16-20]. This work has demonstrated that MRO can change with processing conditions [18, 19], even when the structure factor $S(k)$ remains unchanged [20].

To appear in

Fall 2003 MRS Meeting, Symposium MM - *Amorphous and Nanocrystalline Metal*

Mat. Res. Soc. Symp. Proc. Vol. 806

Contact email: wgstratton@wisc.edu

FEM measurements in conjunction with computer structural modeling have led to the proposal that the continuous random network (the covalent equivalent of dense random packing) does not adequately represent the structure of real amorphous thin films. Instead, they have a paracrystalline structure [20] consisting of nanometer-sized crystalline grains (MRO) in a more disordered matrix. If the $\text{Al}_{92}\text{Sm}_8$ nucleation site is a form of nanoscale structural order, then we anticipate these amorphous alloys will have a similarly heterogeneous nanoscale structure.

The first FEM measurements on amorphous metals have recently been reported by Hufnagel *et al.* [21, 22]. They have shown that there is a measurable FEM signature in amorphous $\text{Zr}_{57}\text{Ti}_{15}\text{Cu}_{20}\text{Ni}_8\text{Al}_{10}$ which can be modified by adding Ta [21]. They also report that high energy ion milling during TEM sample thinning can introduce artifacts in both FEM and high-resolution electron microscopy measurements [22].

EXPERIMENT

We have studied $\text{Al}_{92}\text{Sm}_8$ amorphous alloy. While other high Al-content alloys are better glass formers and show higher tensile strengths, $\text{Al}_{92}\text{Sm}_8$ amorphous alloy is an excellent model system. It is well studied, contains only two components, and can be made by both cold-rolling and melt-spinning. For this study, melt-spun samples were prepared using a single copper wheel melt spinner at a tangential wheel speed of 55 m/s. Cold-rolled specimens were made using an automatic rolling mill, with 200 roll and fold passes to a total true strain of 0.69 at an average strain rate of $\sim 0.003 \text{ s}^{-1}$. TEM samples were prepared by stamping the alloy into 3 mm diameter disks and electropolishing with a Struers TenuPol-5 electropolisher in an electrolyte of 25 vol. % nitric acid solution (assay 69.8%) and 75 vol. % methanol at $-55 \text{ }^\circ\text{C}$. Ion milling was avoided because it may produce artifacts in $V(k)$ [22].

Previous experiments with $\text{Al}_{88}\text{Y}_7\text{Fe}_5$ amorphous alloy showed that thinned TEM samples may structurally age with time. $V(k)$ for a TEM sample left at room temperature in a vacuum desiccator for several weeks showed significant differences compared to $V(k)$ of a freshly thinned TEM sample. All specimens discussed here were viewed within 48 hours of thinning. Bulk source materials and thinned specimens were kept in a freezer when not in use.

Annealing experiments below the crystallization temperature were conducted in a vacuum oven. Results reported here are for melt-spun ribbons annealed for 6 hours at $130 \text{ }^\circ\text{C}$ in 2 Torr of air. This is similar to conditions used in microcalorimetry experiments that showed heat evolution of 0.19 J [12]. Samples devitrified during annealing treatments at $130 \text{ }^\circ\text{C}$ showed a decrease in both the nucleation and growth rate of Al crystallites, indicating that the as-quenched matrix undergoes some form of relaxation that acts to exhaust catalytic nucleation [12].

FEM measurements were performed on a LEO 912 EFTEM at 120 kV accelerating voltage and a spatial resolution of 16 Å. Each $V(k)$ curve represents the average of measurements from at least 9 areas of the specimen, quoted with one standard deviation of the mean error bars. The total sample area measured for each curve was $\sim 0.13 \mu\text{m}^2$. The thickness of each area was measured by determining the average electron transmittance through a small objective aperture. Measured $V(k)$ will change with sample thickness [23], so only areas with $>60\%$ transmittance were selected. We estimate that this represents a physical sample thickness $<40 \text{ nm}$, although this has not been independently measured. Images were processed as previously described [23]. Care was taken to avoid the automatic 16 bit to 8 bit TIFF conversion

To appear in

Fall 2003 MRS Meeting, Symposium MM - *Amorphous and Nanocrystalline Metal*

Mat. Res. Soc. Symp. Proc. Vol. 806

Contact email: wgstratton@wisc.edu

in the AnalySIS ESIvision image acquisition software used, as this will generate spurious peaks in $V(k)$.

RESULTS AND DISCUSSION

Melt-spun and cold-rolled specimens of $\text{Al}_{92}\text{Sm}_8$ are not generally homogeneously amorphous so we used selected area diffraction in the TEM to ensure that all the areas we imaged were diffraction amorphous. Typical electron diffraction data are shown in Figure 1. Low temperature annealing on the melt-spun material has no visible effect on the electron diffraction pattern from the as-spun melt-spun material. The cold-rolled specimen also has a fully amorphous electron diffraction pattern, but the peaks occur in different places than the melt spun samples. This indicates some difference in short-range order between the two samples, despite their nominally similar composition. More sophisticated electron diffraction experiments to determine the electron radial distribution function [24] are underway to understand this difference.

Figure 2 shows $V(k)$ data for all three samples. While the as-prepared and annealed melt-spun samples show peaks in $V(k)$ at $k = 0.58 \text{ 1/\AA}$ and 0.80 1/\AA respectively, the peaks are too broad to be attributed to a particular Bragg reflection in the Al-Sm system. The as-spun sample has the highest peaks in $V(k)$, indicating that it has the most MRO. The smaller peaks in the annealed melt-spun sample indicate that this MRO is reduced by low-temperature annealing. The peaks remain in the same position, indicating that the nature or type of MRO remains unchanged. These results show that there is measurable MRO in $\text{Al}_{92}\text{Sm}_8$ amorphous alloy, and that the MRO we measure with FEM is modified by the same annealing treatment that changes the crystallization behavior. This data does not explicitly show that the MRO measured are the nucleation sites, but the fact that they both change with low temperature thermal annealing implies that they are related.

$V(k)$ for the cold-rolled sample is dramatically different. As shown in Figure 2, the cold-rolled sample shows one large peak at $k = 0.32 \text{ 1/\AA}$, where no peak is present in the melt-spun data. In the range of k where the

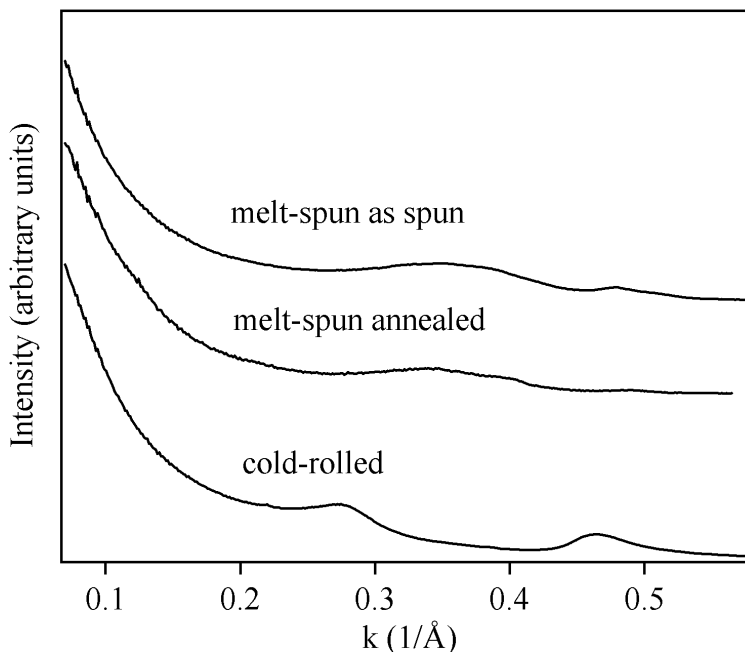


Figure 1. The annular average of typical diffraction patterns from the $\text{Al}_{92}\text{Sm}_8$ amorphous alloy samples produced by cold-rolling and melt-spinning before and after a low temperature anneal. The curves have been shifted vertically for clarity. All samples are fully amorphous, and annealing has no visible effect on the melt-spun diffraction pattern.

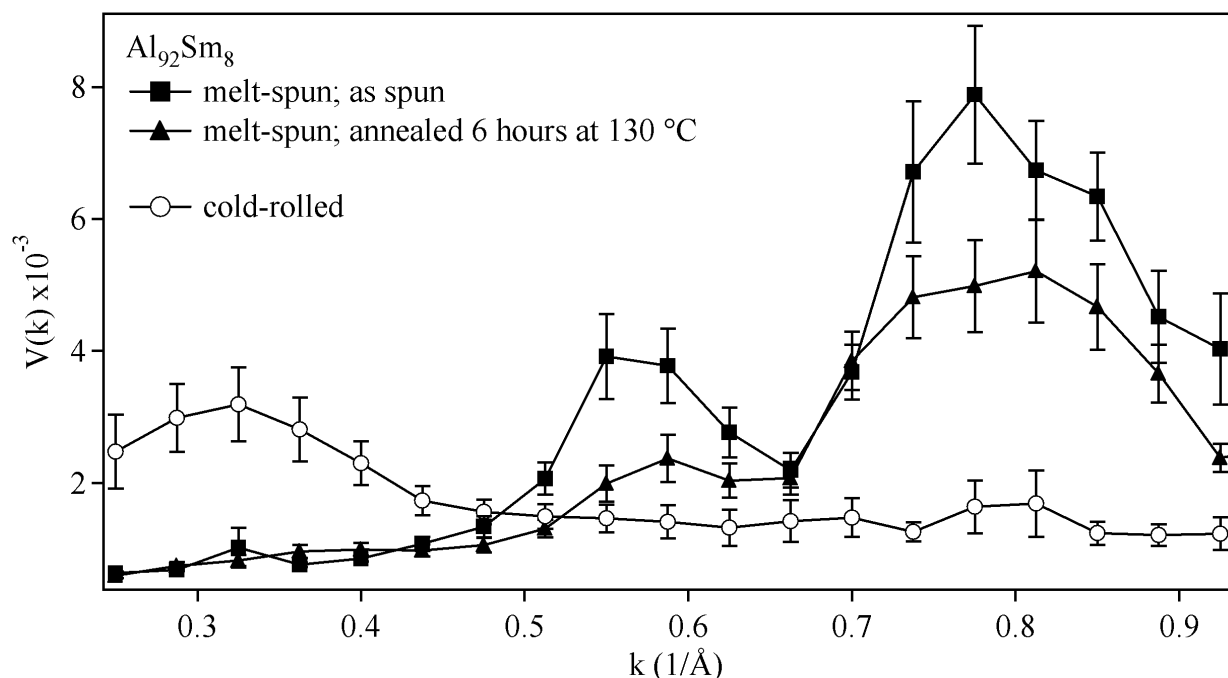


Figure 2. $V(k)$ for melt-spun as-spun, melt-spun annealed, and cold-rolled $\text{Al}_{92}\text{Sm}_8$ amorphous alloy. The peak locations in the as-spun and annealed samples are the same, showing that the same type of MRO is present in both samples. The height of the peaks decreases, indicating a decrease in the degree of MRO. The cold-rolled samples shows a lower peak in a different location, indicating it has less MRO of a different type than the either melt-spun sample.

melt-spun sample shows peaks, the cold-rolled $V(k)$ is nearly flat. Further experiments and better statistics are required to determine if the small feature near $k = 0.80 \text{ 1/\AA}$ is significant. The difference in peak location implies that the melt-spun and cold-rolled specimens contain different types of nanoscale structure. The lower magnitude of the peak in the cold-rolled sample suggests that whatever the form of MRO, it is less pronounced than in the melt-spun samples. The difference in MRO between these two processing techniques may be connected to the difference in crystallization behavior.

These preliminary results are intriguing, but not conclusive. Additional work is underway exploring further the annealing and processing parameter space for both the melt-spun and cold-rolled amorphous alloy, including annealing time and temperature, wheel speed, strain rate, and total strain. Understanding the origin of the peaks in $V(k)$ in terms of a particular atomistic structural motif will require computer modeling of the candidate structures followed by simulations of the FEM signal.

CONCLUSIONS

We have used fluctuation electron microscopy to measure medium-range order in $\text{Al}_{92}\text{Sm}_8$ amorphous alloy as a function of preparation method and annealing below the crystallization temperature. Our preliminary results show that the degree of MRO in melt-spun samples is modified by low temperature annealing which is similar to treatments known to change the samples' recrystallization behavior [12]. Melt-spun and cold-rolled samples with the

same nominal composition have different short-range and medium-range structure. This implies that the MRO we have measured with FEM is connected to the devitrification behavior of this alloy and may be a precursor to primary crystallization.

ACKNOWLEDGEMENTS

W.G.S. and P.M.V. acknowledge the University of Wisconsin – Madison for financial support. J.H. and J.H.P. acknowledge the Army Research Office (DAAD 19-01-1-0486 and DAAD 19-02-1-0245) for financial support. We thank the Applied Superconductivity Center at the University of Wisconsin – Madison for use of their automatic rolling mill.

REFERENCES

1. A. Inoue, K. Ohtera, A. P. Tsai, and T. Masumoto, *Jpn. J. Appl. Phys.* **27**, L479 (1988).
2. Y. He, S. J. Poon, and G. J. Shiflet, *Science* **241**, 1640 (1988).
3. M. Blank-Bewersdorff, *J. Mat. Sci. Lett.* **10**, 1225 (1991).
4. J. C. Foley, D. R. Allen, and J. H. Perepezko, *Scripta Mat.* **35**, 655 (1996).
5. G. Wilde, H. Sieber, and J. H. Perepezko, *Scripta Mat.* **40**, 779 (1999).
6. A. Inoue, *Prog. Mat. Sci.* **43**, 365 (1998).
7. A. Inoue, *Mater. Trans. JIM* **36**, 909 (1992).
8. H. Sieber, G. Wilde, A. Sagel, and J. H. Perepezko, *J. Non-Cryst. Sol.* **A301**, 250 (1999).
9. K. Nakazato, Y. Kawamura, A. P. Tsai, and A. Inoue, *Appl. Phys. Lett.* **63**, 2644 (1993).
10. A. K. Gangopadhyay, T. K. Croat, and K. F. Kelton, *Acta Mater.* **48**, 4035 (2000).
11. K. F. Kelton, T. K. Croat, A. K. Gangopadhyay, L.-Q. Xing, A. L. Greer, M. Weyland, X. Li, and K. Rajan, *J. Non-Cryst. Sol.* **317**, 71 (2003).
12. J. H. Perepezko, W. S. Tong, J. Hamann, R. J. Hebert, H. R. Rösner, and G. Wilde, in *Supercooled Liquids, Glass Transition, and Bulk Metallic Glasses*, edited by T. Egami, A. L. Greer, A. Inoue and S. Ranganathan, (Materials Research Society **754**, Boston, 2002) p. CC10.3.1.
13. M. M. J. Treacy and J. M. Gibson, *Acta Cryst. A* **52**, 212 (1996).
14. P. M. Voyles, J. M. Gibson, and M. M. J. Treacy, *J. Electron Microsc.* **49**, 259 (2000).
15. J. M. Gibson, M. M. J. Treacy, and P. M. Voyles, *Ultramicroscopy* **83**, 169 (2000).
16. J. M. Gibson and M. M. J. Treacy, *Phys. Rev. Lett.* **78**, 1074 (1997).
17. P. M. Voyles, J. E. Gerbi, M. M. J. Treacy, J. M. Gibson, and J. R. Abelson, *Phys. Rev. Lett.* **86**, 5514 (2001).
18. P. M. Voyles and J. R. Abelson, *Solar Energy Materials and Solar Cells* **78**, 85 (2003).
19. P. M. Voyles, J. E. Gerbi, M. M. J. Treacy, J. M. Gibson, and J. R. Abelson, *J. Non-Cryst. Sol.* **293-295**, 45 (2001).
20. M. M. J. Treacy, J. M. Gibson, and P. J. Keblinski, *J. Non-Cryst. Sol.* **231**, 99 (1998).
21. T. C. Hufnagel, C. Fan, R. T. Ott, J. Li, and S. Brennan, *Intermetallics* **10**, 1163 (2002).
22. J. Li, X. Gu, and T. C. Hufnagel, *Microsc. Microanal.* **9**, 509 (2003)
23. P. M. Voyles, M. M. J. Treacy, J. M. Gibson, H.-C. Jin, and J. R. Abelson, in *Advances in Materials Problem Solving with the Electron Microscope*, edited by I. Petrov, (Materials Research Society **589**, 1999) p. 155.
24. D. J. H. Cockayne and D. R. McKenzie, *Acta Cryst.* **A44**, 870 (1988).